

# *Satellite evidence for China's leading role in restoring vegetation productivity over global karst ecosystems*

Article

Accepted Version

Creative Commons: Attribution-Noncommercial-No Derivative Works 4.0

Tang, X., Xiao, J., Ma, M., Yang, H. ORCID: <https://orcid.org/0000-0001-9940-8273>, Li, X., Ding, Z., Yu, P., Zhang, Y., Wu, C., Huang, J. and Thompson, J. R. (2022) Satellite evidence for China's leading role in restoring vegetation productivity over global karst ecosystems. *Forest Ecology and Management*, 507. 120000. ISSN 0378-1127 doi: 10.1016/j.foreco.2021.120000 Available at <https://centaur.reading.ac.uk/104659/>

It is advisable to refer to the publisher's version if you intend to cite from the work. See [Guidance on citing](#).

To link to this article DOI: <http://dx.doi.org/10.1016/j.foreco.2021.120000>

Publisher: Elsevier

All outputs in CentAUR are protected by Intellectual Property Rights law, including copyright law. Copyright and IPR is retained by the creators or other copyright holders. Terms and conditions for use of this material are defined in the [End User Agreement](#).

[www.reading.ac.uk/centaur](http://www.reading.ac.uk/centaur)

## **CentAUR**

Central Archive at the University of Reading

Reading's research outputs online

# Satellite evidence for China's leading role in restoring vegetation productivity over global karst ecosystems

Xuguang Tang <sup>a, b, \*</sup>, Jingfeng Xiao <sup>c</sup>, Mingguo Ma <sup>a, b, \*</sup>, Hong Yang <sup>d</sup>, Xing Li <sup>c</sup>, Zhi Ding <sup>a, b</sup>, Pujia Yu <sup>a, b</sup>, Yongguang Zhang <sup>e</sup>, Chaoyang Wu <sup>f</sup>, Jing Huang <sup>a, b</sup>, Julian R. Thompson <sup>g</sup>

<sup>a</sup> *Chongqing Jinpo Mountain Karst Ecosystem National Observation and Research Station, School of Geographical Sciences, Southwest University, Chongqing 400715, China*

<sup>b</sup> *Chongqing Engineering Research Center for Remote Sensing Big Data Application, Southwest University, Chongqing 400715, China*

<sup>c</sup> *Earth Systems Research Center, Institute for the Study of Earth, Oceans, and Space, University of New Hampshire, Durham, NH 03824, USA*

<sup>d</sup> *Department of Geography and Environmental Science, University of Reading, Whiteknights, Reading RG6 6AB, UK*

<sup>e</sup> *International Institute for Earth System Sciences, Nanjing University, Nanjing 210023, China*

<sup>f</sup> *The Key Laboratory of Land Surface Pattern and Simulation, Institute of Geographical Sciences and Natural Resources Research, Chinese Academy of Sciences, Beijing 100101, China*

<sup>g</sup> *Department of Geography, University College London, London WC1E 6BT, UK*

\* Corresponding authors at: Chongqing Jinpo Mountain Karst Ecosystem National Observation and Research Station, School of Geographical Sciences, Southwest University, Chongqing 400715, China.

E-mail addresses: xgtang@swu.edu.cn (X. Tang), mmg@swu.edu.cn (M. Ma).

## Abstract

Karst ecosystems occupy approximately 20% of the Earth's land surface with the unique and vulnerable geomorphological and hydrogeological characteristics. To date, it remains a challenge to accurately monitor ecosystem productivity from space, as well as their responses to the environmental conditions due to climate change and anthropogenic pressure, which is pivotal to the sustainable development strategies in global karst areas. Here we use a reconstructed long-term solar-induced chlorophyll fluorescence dataset (SIF) and two satellite-based gross primary productivity (GPP) products to examine the patterns and trends of vegetation productivity within global karst ecosystems, and to assess the relative contributions of different countries to the restoration of these fragile ecosystems over the period 2001–2016. As an effective proxy for terrestrial GPP, SIF reveals a greening trend across most of the world's karst areas. China and the European Union (EU) lead the world in vegetation greening within their karst areas by 78.02% and 42.44%, respectively. The total net increase in SIF shows that China alone accounted for 43.66% with just 7.0% of global karst area. Brazil is the only country with a negative greening trend. Recent land cover changes caused by the grain-for-green programme in China and deforestation in Brazil account for 36.93% and 64.71% of the increases and decreases, respectively. Our results have significant implications for restoring ecosystem productivity in global karst areas.

## 1. Introduction

Global environmental change has rapidly altered terrestrial vegetation, with consequent impacts on the functioning of the Earth system and the provision of ecosystem services (Grimm et al., 2013). Long-term changes in vegetation can be attributed to multiple interacting factors including changes in climate and anthropogenic activities, particularly land use and land cover changes (Piao et al., 2015; Mao et al., 2016; Keenan and Riley, 2018). Despite the observed greening of many parts of the globe derived from a range of satellite data over the last decade (Ju & Masek, 2016; Zhu et al., 2016), uncertainties still remain regarding the dominant controls of the trends, the spatial differences, and the possibility of continued greening in face of future environmental change. In particular, the responses of the world's ecologically-fragile areas, including karst ecosystems, to the changing environmental conditions are not well understood.

Karst landscapes, characterized by features such as caves, sinkholes and extensive underground water flow systems developed on predominantly limestone geologies, link the Earth's surface to the subsurface (De Waele et al., 2015; Yang et al., 2020). Approximately 25% of the world population depends upon natural resources and ecosystem services derived from karst ecosystems (Ford & Williams, 2007). Given the large extent and wide distribution of karst terrain around the world (Fig. S1), these ecosystems play important roles in regulating the terrestrial carbon cycle and potentially mitigating climate change. However, rocky desertification has emerged as one of the most serious environmental problems in karstic areas because of long-term over-exploitation. It is a process of land degradation involving serious soil erosion, extensive exposure of underlying rocks, drastic declines in soil productivity, and the appearance of a desert-like landscape. The occurrence and magnitude of these environmental changes vary around the world. Of the three largest global karst regions, the eastern North America and middle and southern parts of Europe are relatively unaffected. In contrast, the large karst area of East Asia has seen widespread rocky desertification and is now recognized as an ecologically-fragile region. Appropriate management strategies to prevent and control the expansion of rocky desertification are critically necessary for the sustainable development of global karst ecosystems. Several countries including China have implemented large-area ecological conservation projects to combat desertification and improve ecological conditions (Tong et al., 2018; Laffoon et al., 2015). Long-term management of such initiatives requires accurate monitoring of restoration progress.

Several different approaches have been used to monitor the variability in terrestrial gross primary productivity (GPP) including satellite-derived vegetation indices, light-use efficiency models and process-based models (Piao et al., 2015; Zhu et al., 2016; Wu et al., 2018). However, these methods are often associated with large discrepancies due to uncertainties in model algorithm or input data (Guanter et al., 2014). Alternatively, satellite observations of solar-induced chlorophyll fluorescence (SIF), particularly from the Orbiting Carbon Observatory-2 (OCO-2) mission, provide a novel proxy for GPP across multiple spatiotemporal scales. These data are valuable for studying ecosystem dynamics and carbon-climate feedbacks (Walther et al., 2016; Sun et al., 2017). However, the spatially and temporally sparse SIF retrievals for OCO-2 constrain their applications from regional to global scales. The development of a global spatially contiguous SIF dataset with finer resolution offers the possibility of accurately and repeatedly monitoring terrestrial photosynthesis and ecosystem productivity at various spatiotemporal scales (Zhang et al., 2018; Li & Xiao, 2019). Here, we use a new globally, reconstructed OCO-2 based SIF dataset (GOSIF) from 2001 to 2016, together with two widely-used satellite-based GPP products, to (1) analyze the spatial patterns and trends in productivity of the world's karst ecosystems; (2) investigate the progress of different countries in restoring these fragile ecosystems; and (3) assess the prominent environmental controls on the observed trends that include both climatic factors and land cover change. Fig. S2 briefly described the framework of this study.

## 2. Methods and materials

### 2.1. Global OCO-2 based SIF dataset

The advent of satellite-derived SIF data promises a new era in monitoring terrestrial ecosystems. Recent studies have confirmed that SIF retrieval from the Orbiting Carbon Observatory-2 (OCO-2) provide a powerful proxy for terrestrial GPP at multiple spatiotemporal scales (Sun et al., 2017, Li et al., 2018). However, the spatially and temporally sparse nature of OCO-2 data makes it challenging for the applications from the ecosystem level to the globe. Thus, we used a new global, 0.05° SIF data set (GOSIF) at an 8-day interval derived from OCO-2, MODIS and MERRA-2 data (Li & Xiao, 2019). These SIF estimates were found to be significantly correlated with GPP data from 91 FLUXNET sites ( $R^2 = 0.73$ ,  $p < 0.001$ ). Compared with the coarse-resolution SIF data directly aggregated from discrete OCO-2 soundings, GOSIF has the advantages of finer spatial resolution, globally continuous coverage and a much longer period. It is thus effective for assessing terrestrial photosynthesis and ecosystem function. More details of the methodology, validation, and spatiotemporal characteristics of this product can be found in the reference (Li & Xiao, 2019). In this study, we used the time-series GOSIF dataset from 2001 to 2016 ([http://data.globalecology.unh.edu/data/GOSIF\\_v2/](http://data.globalecology.unh.edu/data/GOSIF_v2/)) to analyze long-term vegetation changes in global karst ecosystems. The annual mean SIF for each grid cell was derived from all the 8-day values within each year. Multi-year SIF averages were compared with MODIS and VPM GPP products.

### 2.2. Site-level observations of SIF

Despite that the satellite-based GOSIF dataset has emerged as a novel and powerful approach for terrestrial vegetation monitoring, its robustness needs to be validated for large-scale applications. Fortunately, several ground-based spectrometer systems have been developed and installed at the eddy covariance (EC) towers in recent years, which provide continuous SIF observations (Magney et al., 2019). In total of four tower sites including one subtropical evergreen forest (CN-HT), one subalpine conifer forest (US-NR) and two temperate cropland were used in this study with available high-frequency SIF retrievals since 2017. The details of instrument specifications, data collection and processing procedures can be found in the literature (Zhang et al., 2021). As shown in Fig. S3, satellite-based SIF generally agreed well with ground-based SIF measurements over a variety of vegetation types. The coefficient of determination ( $R^2$ ) and root mean square error (RMSE) varied across different sites, with  $R^2$  ranging from the minimal of 0.688 at CN-HT to the maximal of 0.874 at US-NR and RMSE ranging from the maximal of  $0.084 \text{ W m}^{-2} \mu\text{m}^{-1} \text{ sr}^{-1}$  at CN-DM to the minimal of  $0.020 \text{ W m}^{-2} \mu\text{m}^{-1} \text{ sr}^{-1}$  at US-NR. Considering that there are still mismatch of the footprint between satellite and ground-based measurements, such direct comparison demonstrated the potential of global OCO-2 based SIF dataset.

### 2.3. MODIS GPP product

The MOD17A2 GPP product is the first operational satellite-driven dataset to repeatedly monitor global vegetation productivity at 1-km resolution and an 8-day interval (Zhao et al., 2005). The dataset is widely used for natural resource and land management, global carbon cycle research, ecosystem status assessment, and environmental change monitoring (Tang et al., 2014). The MOD17 algorithm is based on the light use efficiency (LUE) model that relates vegetation photosynthesis to the amount of photosynthetically active radiation (PAR) absorbed by plants during the growth period. The old MODIS GPP product (C4) was revealed to have considerable uncertainties owing to problems in the data inputs. Zhao et al. (2005) rectified these products by optimizing the data processing methods and modifying key parameters, thereby generating improved GPP estimates (C5.5). The 8-day composite 1-km fraction of photosynthetically active radiation (FPAR) and leaf area index (LAI) data from the MOD15 product were used as the remotely-sensed vegetation property dynamic

inputs to the algorithm. Data gaps in the MODIS LAI/FPAR caused by cloud cover were filled with information from accompanying quality-assessment flags. For the daily meteorological dataset required to drive the algorithm, the 6-h National Center for Environmental Prediction/Department of Energy (NCEP/DOE) reanalysis II data were employed. The associated Biome Parameter Lookup Table (BPLUT) was also updated for different vegetation types. These GPP products over the period 2001–2015 at 8-day, monthly, and annual time steps are currently available from the Numerical Terradynamic Simulation Group (NTSG) of the University of Montana (<http://www.ntsug.umt.edu/project/mod17>).

## **2.4. VPM GPP product**

The Vegetation Photosynthesis Model (VPM) GPP product (V20) is based on an improved LUE model driven by satellite remote sensing data from MODIS and climate data from NCEP Reanalysis II dataset (Zhang et al., 2017). The two main input data comprising the enhanced vegetation index (EVI) and land surface water index (LSWI) in the VPM model were derived from the MOD09A1 (C6) land surface reflectance data with a spatial resolution of 500 m and an 8-day time interval. In addition, the VPM GPP product employed a state-of-the-art vegetation index gap-filling and smoothing algorithm and considered the C<sub>3</sub>/C<sub>4</sub> difference in plant photosynthesis pathways, which solved several critical problems in the main GPP products such as the widely-used MOD17A2. The GPP of each pixel was calculated by area-weighted averaged GPP, which was derived from area fraction maps of C<sub>3</sub>/C<sub>4</sub> plants and land use datasets (MCD12Q1). Across 25 eddy covariance flux tower sites, the VPM GPP estimates showed better accuracy in terms of cross-site variability and interannual variability compared to MOD17 GPP (Wu et al., 2018). In this study, the global VPM GPP products between 2001 and 2016 were used for the auxiliary analysis with a spatial resolution of 0.05°×0.05°. These 8-day, monthly and annual data can be downloaded freely from the website <https://doi.org/10.6084/m9.figshare.c.3789814>.

## **2.5. Temperature and precipitation data**

The Global Land Data Assimilation System (GLDAS) combines satellite and ground-based observations, using advanced surface modeling and data assimilation techniques, in order to generate optimal fields of land surface states and fluxes (Hiroko & Rodell, 2016). At present, GLDAS drives four land surface models (LSM): Noah, Catchment, the Community Land Model (CLM) and the Variable Infiltration Capacity (VIC). GLDAS version 2 has two components: one forced entirely with the Princeton meteorological forcing data (GLDAS-2.0) and the other forced with a combination of model and observation-based datasets (GLDAS-2.1). This study used the Noah LSM-based GLDAS-2.1 data at 0.25° resolution from 2001 to 2016 to reveal the dominant factors influencing the long-term trends in annual mean SIF across global karst ecosystems. The monthly meteorological data are generated through temporal averaging of the 3-h products and can be downloaded via <http://disc.sci.gsfc.nasa.gov/uui/datasets?keywords=GLDAS>. Then, the temperature and precipitation data were synthesized into yearly products (mean annual temperature and annual total precipitation).

## **2.6. CCI land cover data**

A new time series of consistent global land cover data at 300 m spatial resolution from 1992 to 2015 is provided by the European Space Agency known as the Climate Change Initiative Land Cover (CCI-LC) products (V2). These annual products are made available through the following website: <http://maps.elie.ucl.ac.be/CCI/viewer/download.php>. The CCI-LC product used the land cover classification system developed by the United Nations (UN) Food and Agriculture Organization (FAO), with a view of being compatible with the plant functional types used in climate models (Poulter et al., 2015). Several studies have demonstrated that CCI-LC products have the largest overall accuracy when compared with another five global land cover datasets including IGBP DISCover, UMD, GLC, MCD12Q1 and GLCNMO (Yang et al., 2017a, Yang et al., 2017b). This study analyzed the time-series CCI-LC products from 2001 to 2015 to explore the effect of land cover changes on global karst ecosystem

productivity. The land cover classes are grouped into nine IPCC land categories (cropland, forest, grassland, shrubland, sparse vegetation, wetland, settlement, bare area and water) for research purpose.

## 2.7. Trend analysis in global SIF

The long-term trends of annual mean SIF across terrestrial ecosystems in the karst areas were analyzed through the non-parametric Mann-Kendall (M-K) test (Gocic & Trajkovic, 2013). The M-K method provides the possibility of testing for non-linear development in SIF consistently increasing or decreasing, and does not assume a specific distribution for the time-series data and is insensitive to outliers. Because of these advantages, it has been widely used for trend analysis recently (Fensholt et al., 2012). The Theil-Sen method was then used to quantify the magnitude of changes over time. This study assessed the frequency distribution of the trends derived from each pixel in accordance to the significance level ( $p$ -value) of the change (with  $p < 0.01$ ,  $p < 0.05$  and  $p > 0.05$  indicating that the increasing or decreasing trends are very significant, significant and insignificant, respectively). The proportions of the karst areas in the top ten countries/region showing significant greening or browning were also evaluated.

## 2.8. Contribution rates

Using the results of the trend analysis for annual average SIF across global karst areas over the period 2001–2016, the contributions to the restoration of karst ecosystems by countries/region were also assessed. The net changes in SIF for a specific area took into account the effects from both statistically significant greening and browning areas, as well as the magnitudes of trends for each pixel. The areas with statistically insignificant trends were set as zero contribution.

$$C_j = \frac{\sum_{i=1}^n T_{i,j}}{\sum_{j=1}^m \sum_{i=1}^n T_{i,j}} \quad (1)$$

where  $C_j$  is the contribution rate of the country  $j$ ;  $m$  is the number of countries containing karst ecosystems ( $m = 150$  here);  $n$  is the pixels with a statistically significant trend in the country  $j$ ; and  $T_{i,j}$  is the trend of each pixel. This study used percentages to represent the contribution rate of each country to the overall global change.

## 2.9. Spatial correlation analysis

The correlation and partial correlation coefficients were performed to reveal the environmental controls, including the temperate and precipitation, on the inter-annual dynamics of SIF across global karst areas (Wang et al., 2019). The formula of Pearson's correlation coefficient ( $r$ ) was as follows:

$$r_{xy} = \frac{\sum_{i=1}^n (x_i - \bar{x})(y_i - \bar{y})}{\sqrt{\sum_{i=1}^n (x_i - \bar{x})^2} \sqrt{\sum_{i=1}^n (y_i - \bar{y})^2}} \quad (2)$$

where  $n$  is the length of the time series data;  $i$  is the number of year,  $i = 1, 2, \dots, 16$ ; and  $x_i$  ( $y_i$ ) and  $\bar{x}$  ( $\bar{y}$ ) are the values of the  $i$  year and the averages of these years, respectively.

The partial correlation coefficient ( $r_{yz \cdot x}$ ) was calculated to reveal the dominant climate factor controlling the variability in SIF. In this way, when assessing the degree of correlations between SIF and temperature (or precipitation), the effect of precipitation (or temperature) is removed:

$$r_{yz\hat{A}\cdot x} = \frac{r_{yz} - r_{yx}r_{zx}}{\sqrt{(1-r_{yx}^2)(1-r_{zx}^2)}} \quad (3)$$

where  $r_{yz\hat{A}\cdot x}$  represents the partial correlation coefficient between  $y$  and  $z$  without consideration of the impact of  $x$ ; and  $r_{yz}, r_{yx}, r_{zx}$  are the simple correlation coefficients between two variables. Through these analyses, the study identified the dominant environmental controlling factor of each pixel.

### 3. Results

#### 3.1. Trends in vegetation dynamics across global karst areas

The satellite-based SIF data exhibited an overall positive trend for a large proportion of the global karst area since the start of the new millennium (Figs. 1, S4). The mean annual greening trend was equivalent to  $0.0004 \text{ W m}^{-2} \mu\text{m}^{-1} \text{ sr}^{-1} \text{ yr}^{-1}$ . Areas with a significant increase in vegetation SIF ( $p < 0.05$ ) covered approximately 31.1% of global karst ecosystems, of which one fifth was concentrated in China's southwestern karst area, making China one of the largest, spatially coherent region of vegetation restoration (Fig. S5). The majority (78.02%) of China's karst area experienced significant greening trends, with only less than 1.2% experiencing browning (Table 1). The EU also made a large contribution to the global greening, with 42.44% of its karst area experiencing increasing trends in SIF and only 0.35% showing significant declines. Only a few regions ( $\sim 2.7\%$  of the global karst area) were identified as having experienced significant negative change over the study period (Fig. S6). Among the top ten countries/region with the largest extent of karst environment (Table 1), Brazil was the only one exhibiting a larger extent of browning (19.43%) than greening (15.83%).

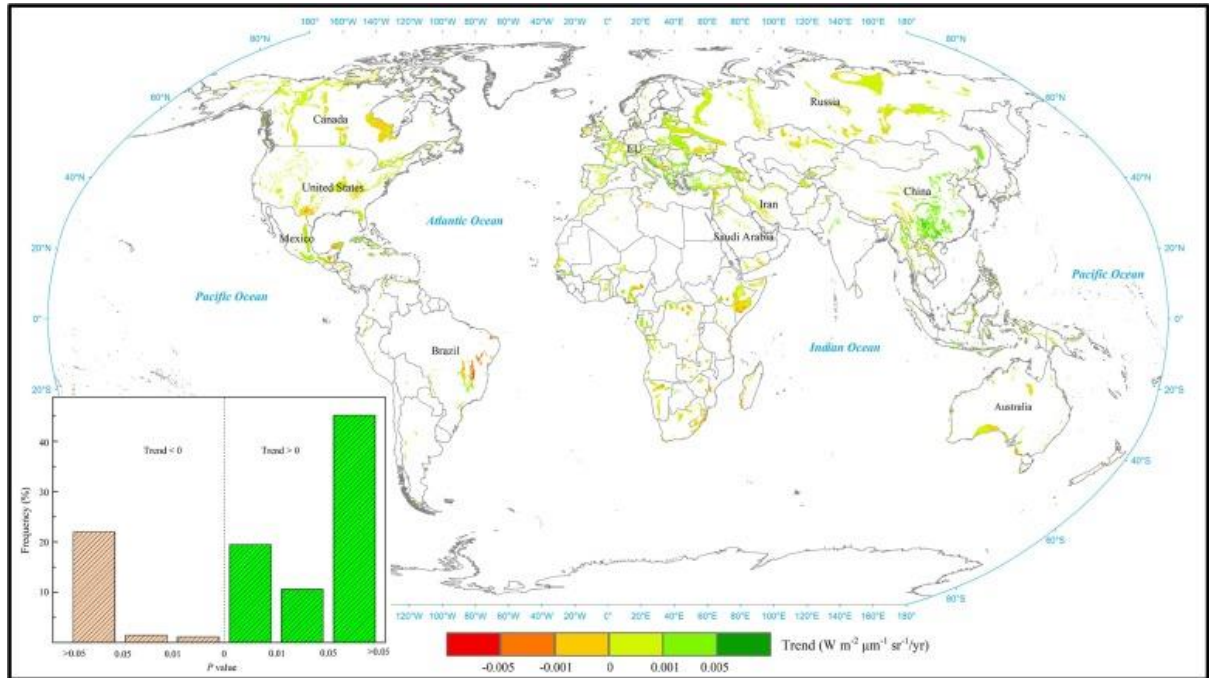


Fig. 1. Spatial trends of annual mean SIF across global karst ecosystems during the period 2001–2016. The frequency distribution of the significance level ( $p$ -value) of the trends is derived using the results for all pixels.



Table 1. Vegetation dynamics in the top ten countries/region (EU) with the world's largest karst areas.

Rank	Country	Karst area (km <sup>2</sup> )	Percentage of total land area	Proportion of areas showing greening	Proportion of areas showing browning	Contribution rate (ranking)
1	Russia	1931825.67	11.5%	25.89%	2.01%	11.82% (3)
2	Canada	1601205.13	16.1%	29.78%	2.81%	6.78% (4)
3	China	1121944.83	11.9%	78.02%	1.14%	43.66% (1)
4	United States	905863.79	9.6%	14.24%	2.56%	2.03% (5)
5	EU	835650.37	19.1%	42.44%	0.35%	11.92% (2)
6	Saudi Arabia	612979.41	31.9%	28.00%	6.98%	0.22% (9)
7	Mexico	606455.46	30.9%	23.03%	2.26%	2.00% (6)
8	Australia	343070.60	4.4%	8.98%	1.10%	0.75% (7)
9	Brazil	271195.98	3.2%	15.83%	19.43%	-1.85% (10)
10	Iran	255116.45	15.7%	30.14%	1.10%	0.71% (8)

Note: The countries of the European Union (EU) are considered together given the large total karst area and relatively small size of some EU countries. Statistics of the proportion of areas showing greening or browning were significant at 0.05 *p*-level.

Vegetation dynamics in global karst area were also examined by comparing the variations in annual mean SIF and GPP (MODIS and VPM) products from 2001 to 2016 (Fig. 2). The annual global mean SIF had a significant increasing trend of  $3.85 \times 10^{-4} \text{ W m}^{-2} \mu\text{m}^{-1} \text{ sr}^{-1} \text{ yr}^{-1}$ . Although global mean VPM GPP exhibited a similar positive trend ( $4.02 \text{ g C m}^{-2} \text{ yr}^{-1}$ ,  $p < 0.001$ ), no significant trend was identified for MODIS GPP ( $p > 0.05$ ). Pearson correlation analysis also showed consistency between the SIF dataset and VPM GPP results ( $p < 0.001$ ,  $r = 0.925$ ) (Fig. S7). Long-term dynamics in the SIF and GPP products over the same period were also evaluated across the top ten countries/region with the largest karst areas (Fig. 3). There were no significant changes for MODIS GPP over all countries, while SIF and VPM GPP generally exhibited similar trends. Despite their large total area, the karst ecosystems in the USA showed no obvious changes in SIF or GPP during the period. In contrast, significant increases were evident for Russia and China. Most notable was the trend in SIF for China's karst vegetation which was nearly five times as large as the global average.

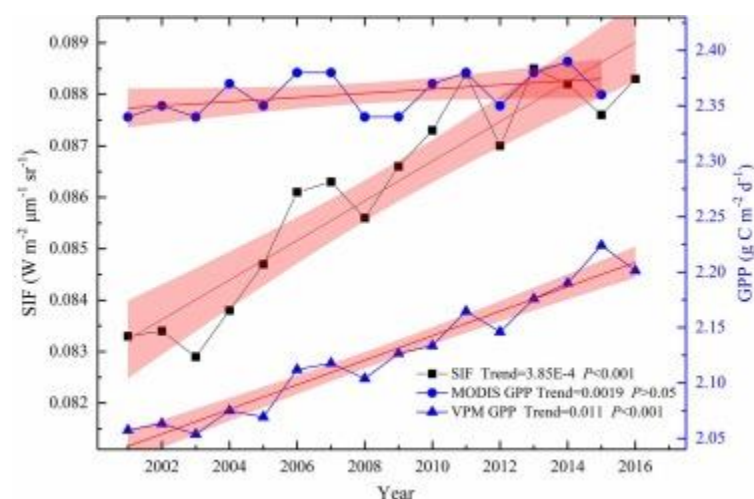


Fig. 2. Long-term dynamics in SIF and GPP (MODIS and VPM) products across global karst area for the period 2001–2016.

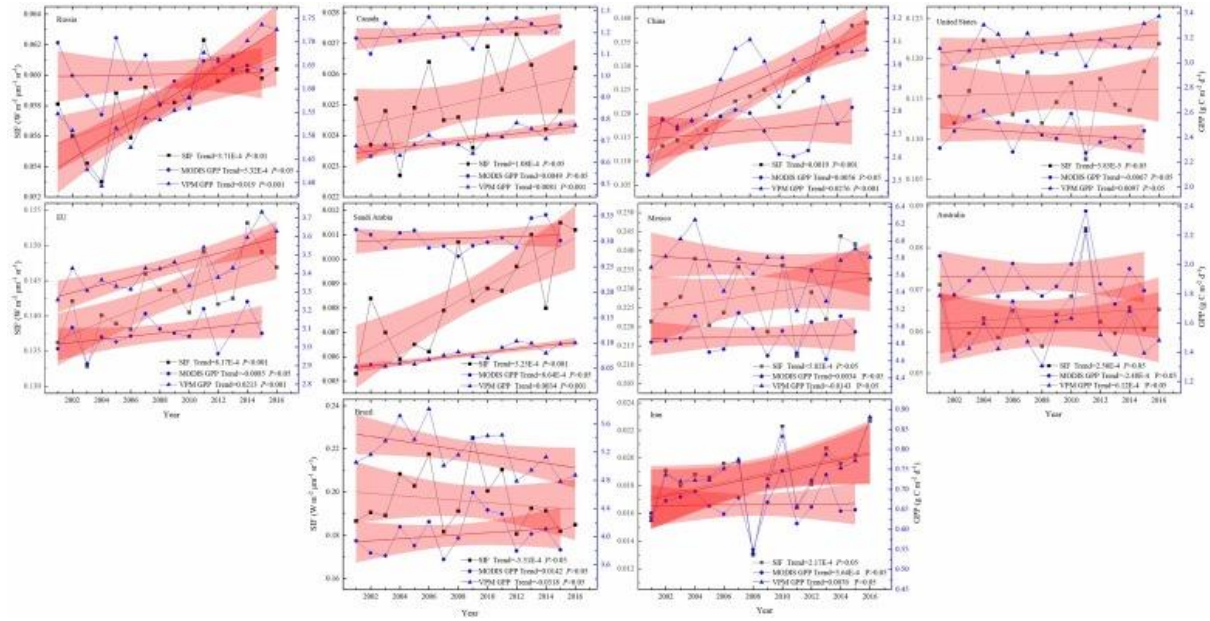


Fig. 3. Long-term dynamics in SIF and GPP (MODIS and VPM) products in the top ten countries/region with the largest karst areas around the world during the period 2001–2016.

### 3.2. Spatial differences in satellite-observed ecosystem productivity across global karst areas

As a direct proxy for vegetation photosynthesis, the satellite-based SIF provides a global perspective on terrestrial GPP across the ecologically-fragile karst regions (Fig. 4). In general, the multi-year mean GOSIF data exhibited strong spatial heterogeneity in gross carbon uptake during the period 2001–2016. The largest SIF values appeared primarily in tropical (e.g. Central Africa, Brazil and Mexico) and subtropical (e.g. Southwest China, Southeast USA) regions. Europe's karst ecosystems also exhibited relatively high SIF. In contrast, most karst areas in the mid- and high latitudes exhibited low SIF values (e.g. West Asia, Russia, Canada, western USA and Australia). Comparison of the spatial patterns of multi-year mean MODIS and VPM GPP products over global karst areas (Fig. 5) demonstrated generally good agreement between state-of-the-art satellite data-driven approaches and the SIF observations. Despite similar global patterns, the GPP estimates from MODIS and VPM varied in magnitude. In general, GPP values derived from VPM were larger than those of the MODIS product for karst areas in the eastern USA, Brazil, southwestern China and Europe. In addition, comparison of satellite-based GPP products with SIF retrievals across the top ten countries/region (i.e. the EU) with the largest karst areas (Fig. 6) demonstrated the consistent performance of the different proxies in monitoring spatial patterns in ecosystem productivity. The largest SIF and GPP values are identified in Mexico and Brazil, followed by the EU, China and USA. In contrast, the smallest are found within the karst areas of predominantly arid/semi-arid Iran and Saudi Arabia.

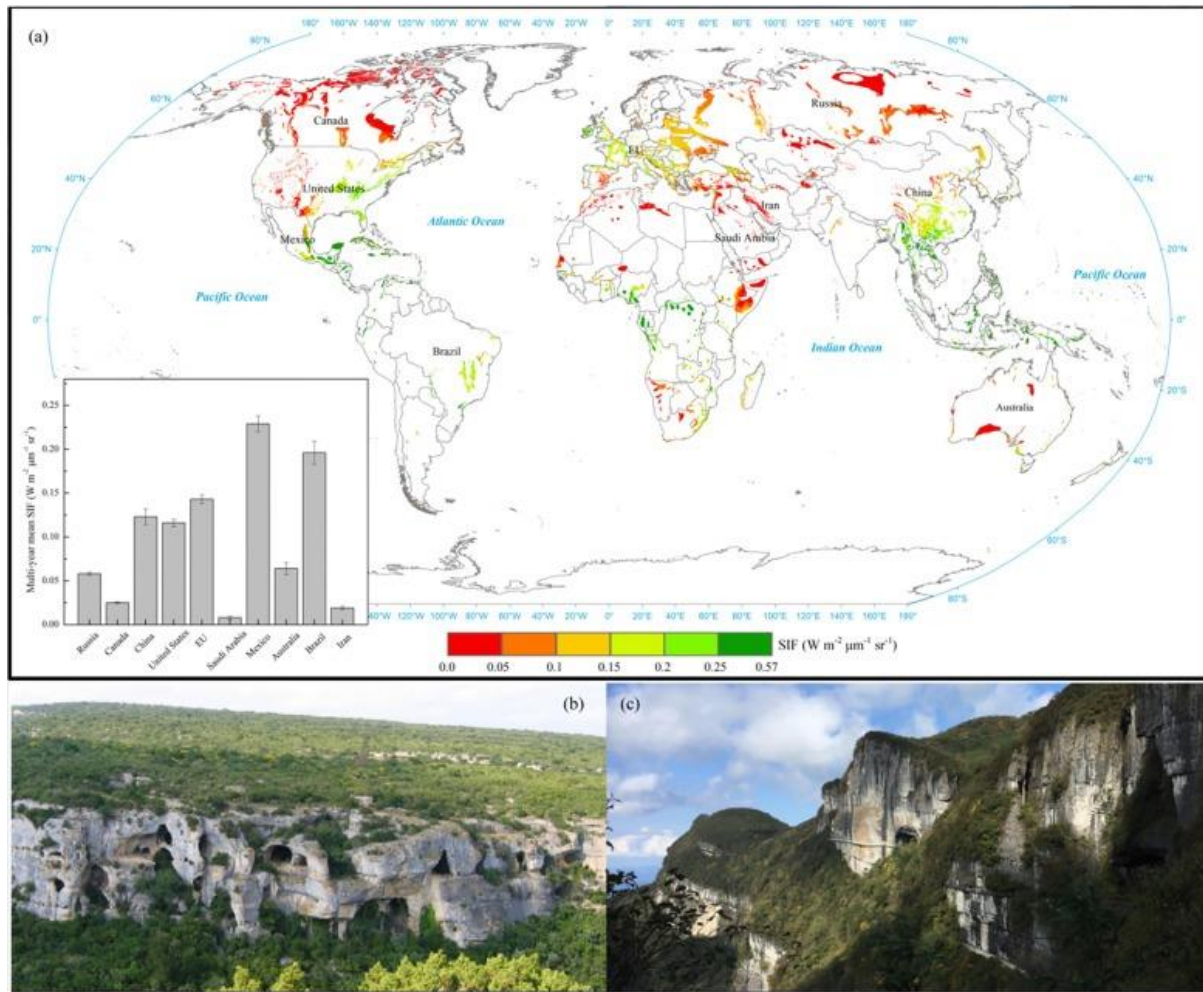


Fig. 4. Spatial patterns of multi-year mean SIF across the world's karst areas during the period 2001–2016 (a) and typical karst landscapes (b and c). Multi-year mean SIF in the top ten countries/region (EU) with the largest karst area around the world are indicated. Error bars are  $\pm 1$  standard error of the mean. The image (b) is Sierra Gorda, Mexico (downloaded from [http://upload.wikimedia.org/wikipedia/commons/e/e9/Karst\\_minerve.jpg](http://upload.wikimedia.org/wikipedia/commons/e/e9/Karst_minerve.jpg).) and image (c) is the Jinfoshan karst area of southwestern China (photographed by Dr. Pingheng Yang, the Research Base of Karst Eco-environments at Nanchuan in Chongqing, Ministry of Nature Resources, Southwest University, China).



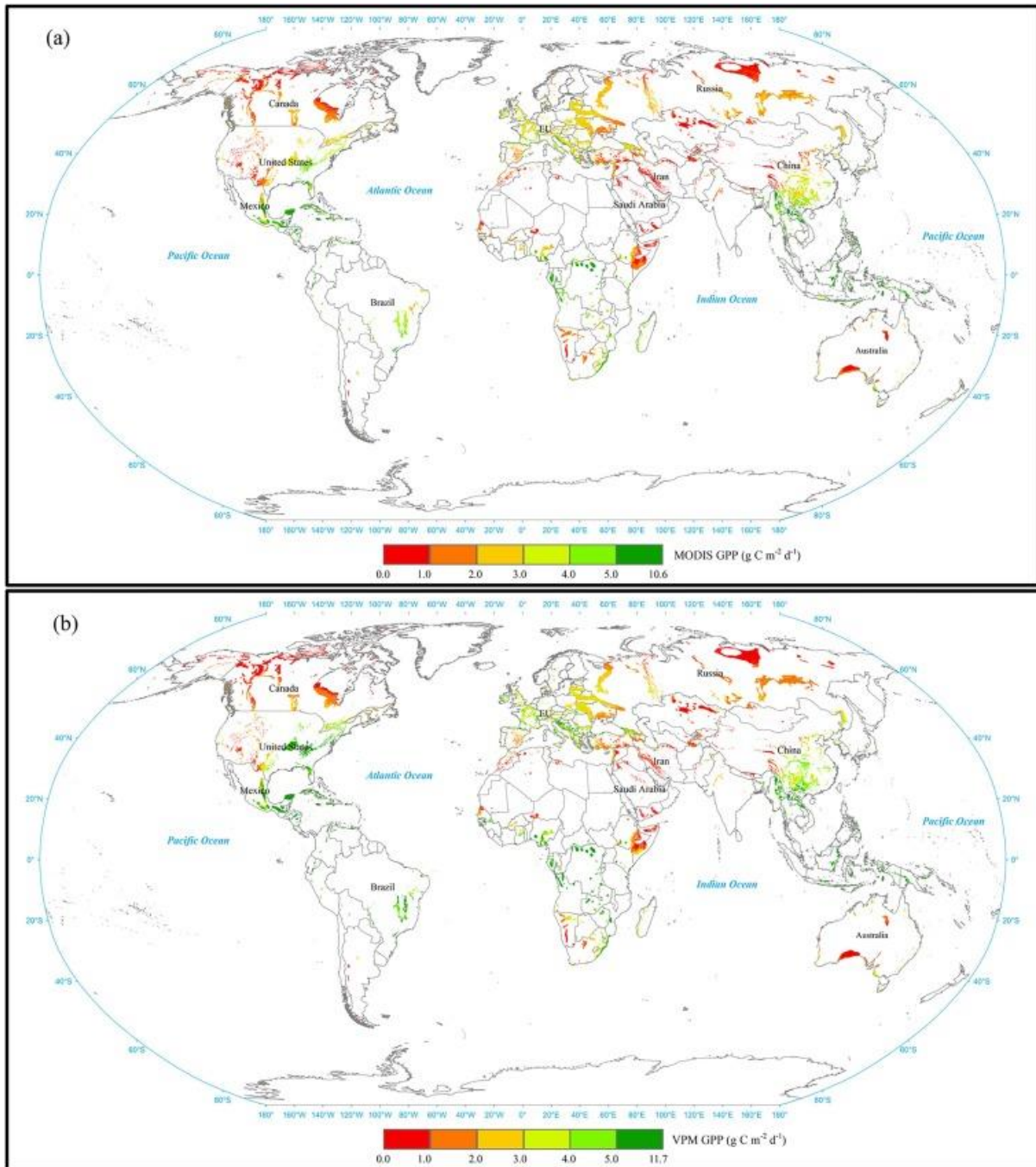


Fig. 5. Magnitude and spatial patterns of multi-year mean MODIS GPP (a) and VPM GPP (b) across terrestrial ecosystems in global karst area.

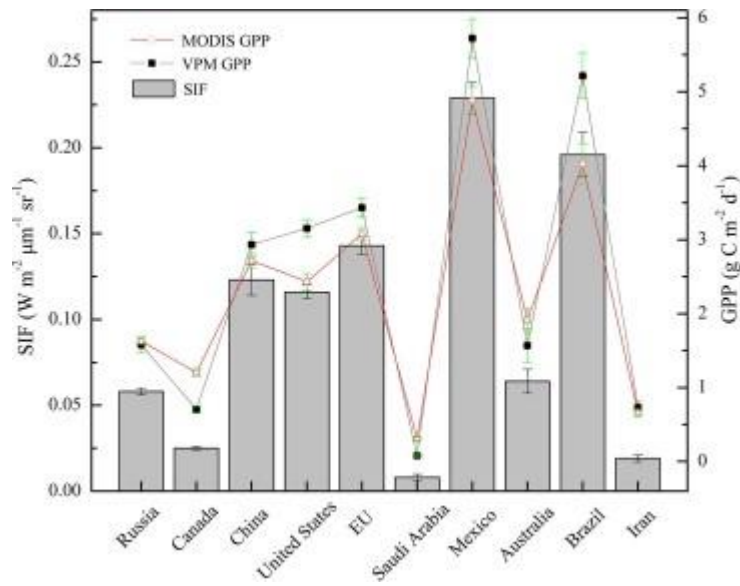


Fig. 6. Multi-year mean SIF and GPP (MODIS and VPM) products in the top ten countries/region with the largest karst areas. Error bars are  $\pm 1$  standard error of the mean.

### 3.3. Contributions to the restoration of global karst ecosystems by country

The absolute contributions to the global net changes were jointly determined by the karst area and magnitude of the changes. On the basis of the trend analysis in annual mean SIF across the karst regions between 2001 and 2016, the contribution rates of each country/region (the EU) to the restoration of ecologically-fragile karst areas are summarized in Fig. 7. Overall, the net increase mainly occurred in the northern hemisphere, while smaller increases and declines in SIF were more concentrated in the southern hemisphere. The top ten countries/region with the largest karst area contributed 78.04% of the global karst vegetation increase (Table 1). Most notably China, which has only 7.0% of the global karst area, accounted for 43.66% of the observed total net change. The EU (11.92%), Russia (11.82%) and Canada (6.78%) also made significant contributions. Although the USA has the fourth largest karst area, its contribution to global net change was only 2.03% (Table 1). Brazil was the only country amongst the top ten with a negative overall contribution (-1.85%).

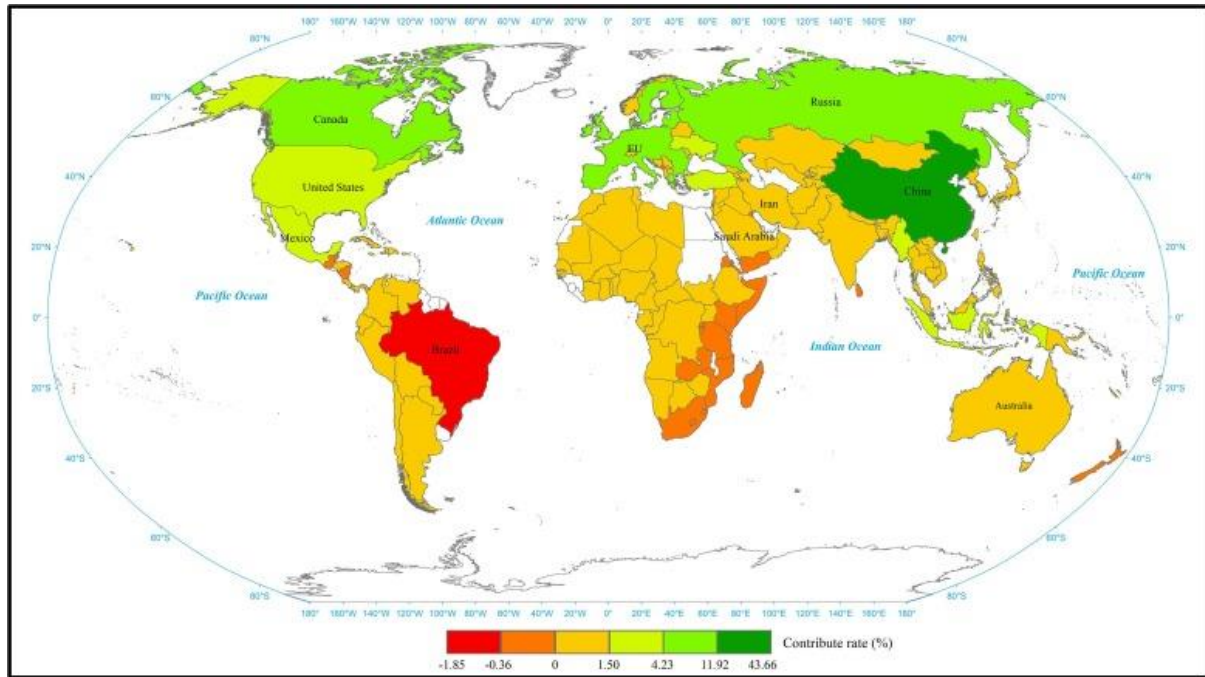


Fig. 7. The contribution rates (%) of each country in restoring global karst ecosystem productivity. The countries of the European Union (EU) are considered together given the large total karst area and relatively small size of some EU countries.

### 3.4. Environmental controls on vegetation restoration

In order to explore the environmental controls on trends in vegetation dynamics across global karst area, we firstly performed a correlation analysis between time-series of SIF and meteorological data (Fig. 8, Fig. 9). The analysis indicated that a large proportion of the changes in world's karst ecosystems were related to temperature and precipitation. More specifically, the area exhibiting significantly positive correlations was over twice as large as that associated with significantly negative correlations. Interestingly, temperature exerted predominantly positive effects in the northern hemisphere and negative effects in the southern hemisphere (e.g. Brazil, South Africa and Australia). Precipitation mainly exhibited negative correlations in high-latitude countries such as Russia and Canada. Partial correlations were also conducted to better understand the dominant environmental controls (Figs. S7 and S8). Results demonstrated spatial variability in the dominance of either temperature or precipitation upon SIF trends (Fig. 10). Approximately 17.26% of the total karst areas was strongly affected by precipitation ( $p < 0.05$ ); 10.70% of the area was obviously impacted by temperature ( $p < 0.05$ ); and only 3.66% of the area was jointly controlled by precipitation and temperature ( $p < 0.05$ ). A clear and consistent trend existed between the changes in precipitation and vegetation across a large portion of the global karst area. The karst area of eastern Canada was the largest spatially coherent region dominated by a positive relationship between temperature and vegetation productivity as indicated by SIF (Figs. 10, S8).

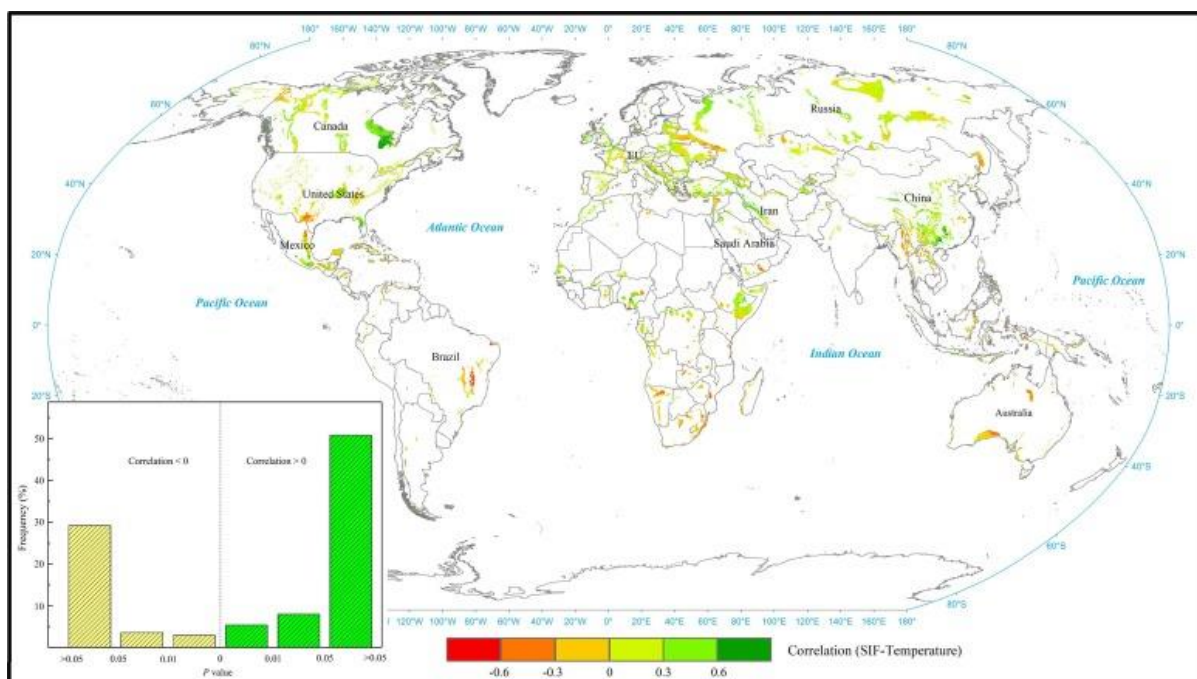


Fig. 8. Spatial correlation analysis of annual mean SIF and temperature across terrestrial karst ecosystems during the period 2001–2016. The frequency distribution of the significance level ( $p$ -value) of the correlations is derived for each pixel.

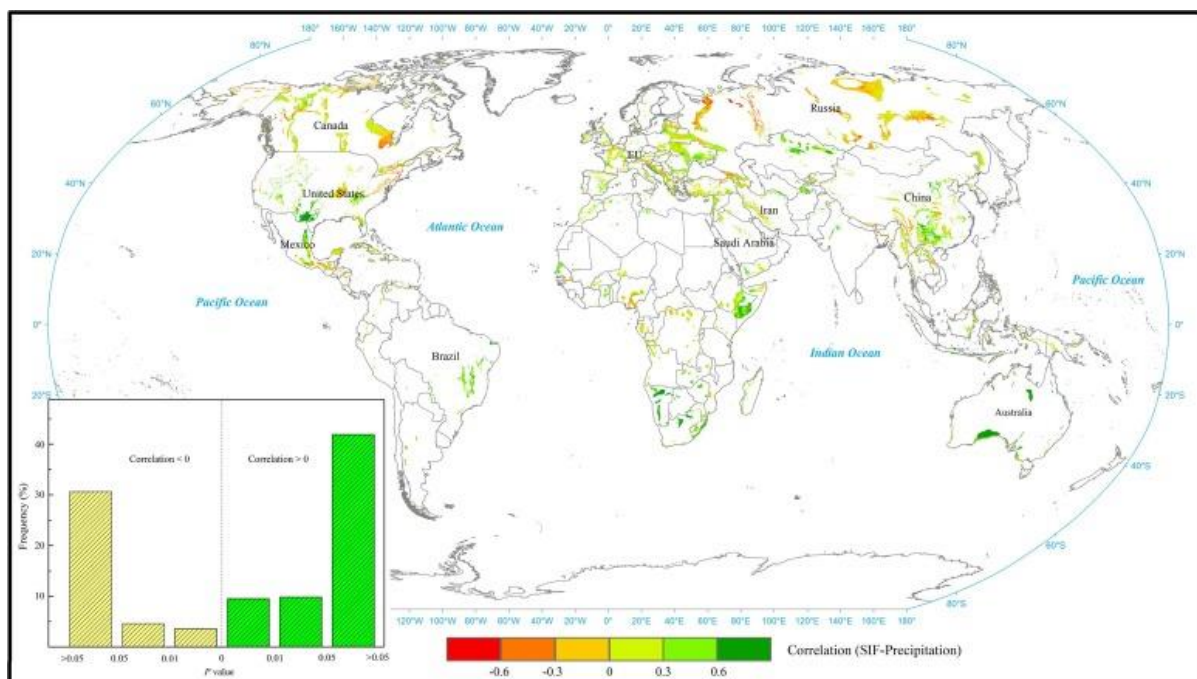


Fig. 9. Spatial correlation analysis of annual mean SIF and precipitation across terrestrial karst ecosystems during the period 2001–2016. The frequency distribution of the significance level ( $p$ -value) of the correlations is derived for each pixel.



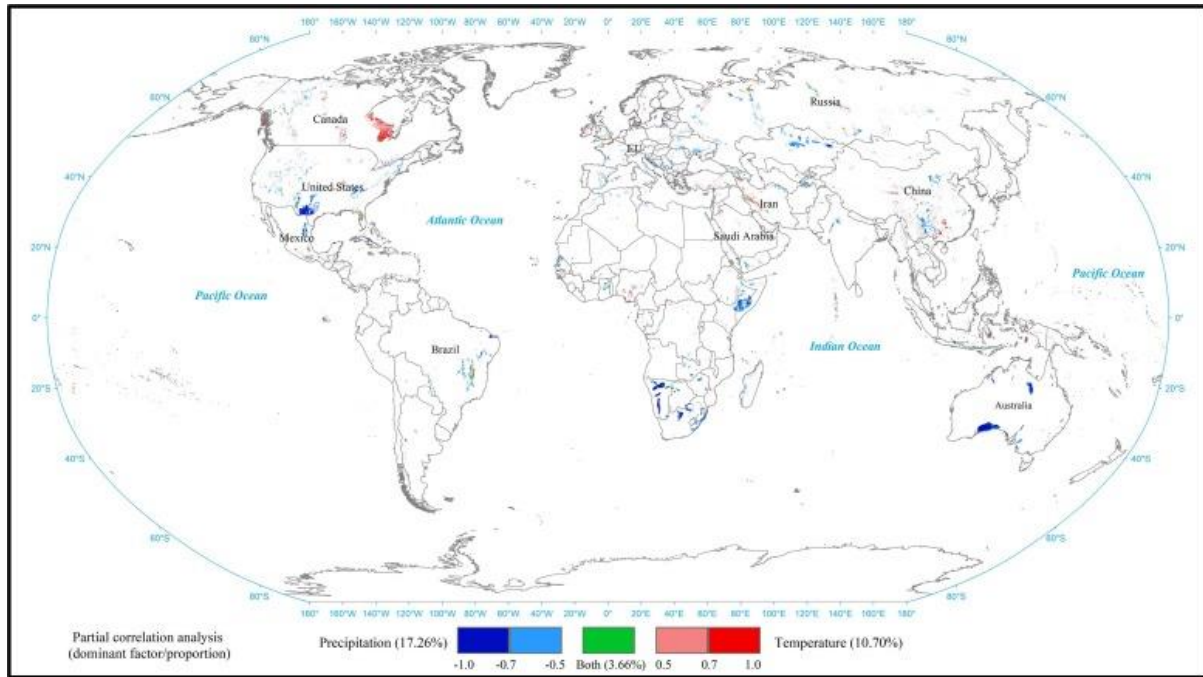


Fig. 10. Dominant climatic factors (precipitation and temperature) controlling long-term trends in annual mean SIF across global karst ecosystems between 2001 and 2016. The partial correlation coefficients between SIF and temperature/precipitation that are significant at the 0.05  $p$ -level are shown. The figure uses the positive and negative values to describe the effects of temperature and precipitation, respectively. The proportions of karst area associated with dominant factors are indicated.

As reported above, the individual contribution of each country to the net increase in SIF for global karst ecosystems varied, ranging between 43.66% (China) and -1.85% (Brazil) for the top ten countries/region (the EU). The study further examined the effect of land cover changes due to human activities on karst areas in these two contrasting countries (Fig. 11). In China, forest, cropland and grassland together occupy over 85.0% of the total karst area (Fig. S9). With the implementation of a number of ecological restoration projects in China since 2001, large-area afforestation and conservation efforts improved the karst vegetation in approximately 45.10% of the regional change (Fig. 11a), which accounted for 36.93% of the increase in terrestrial SIF. In Brazil, forest, shrubland and cropland are the dominant land covers, occupying over 90% of the nation's karst areas (Fig. S10). Over the period 2001–2016, more than half of the land-cover changes were due to deforestation and this accounted for 64.71% of Brazil's decline in SIF for karst ecosystems (Fig. 11b).



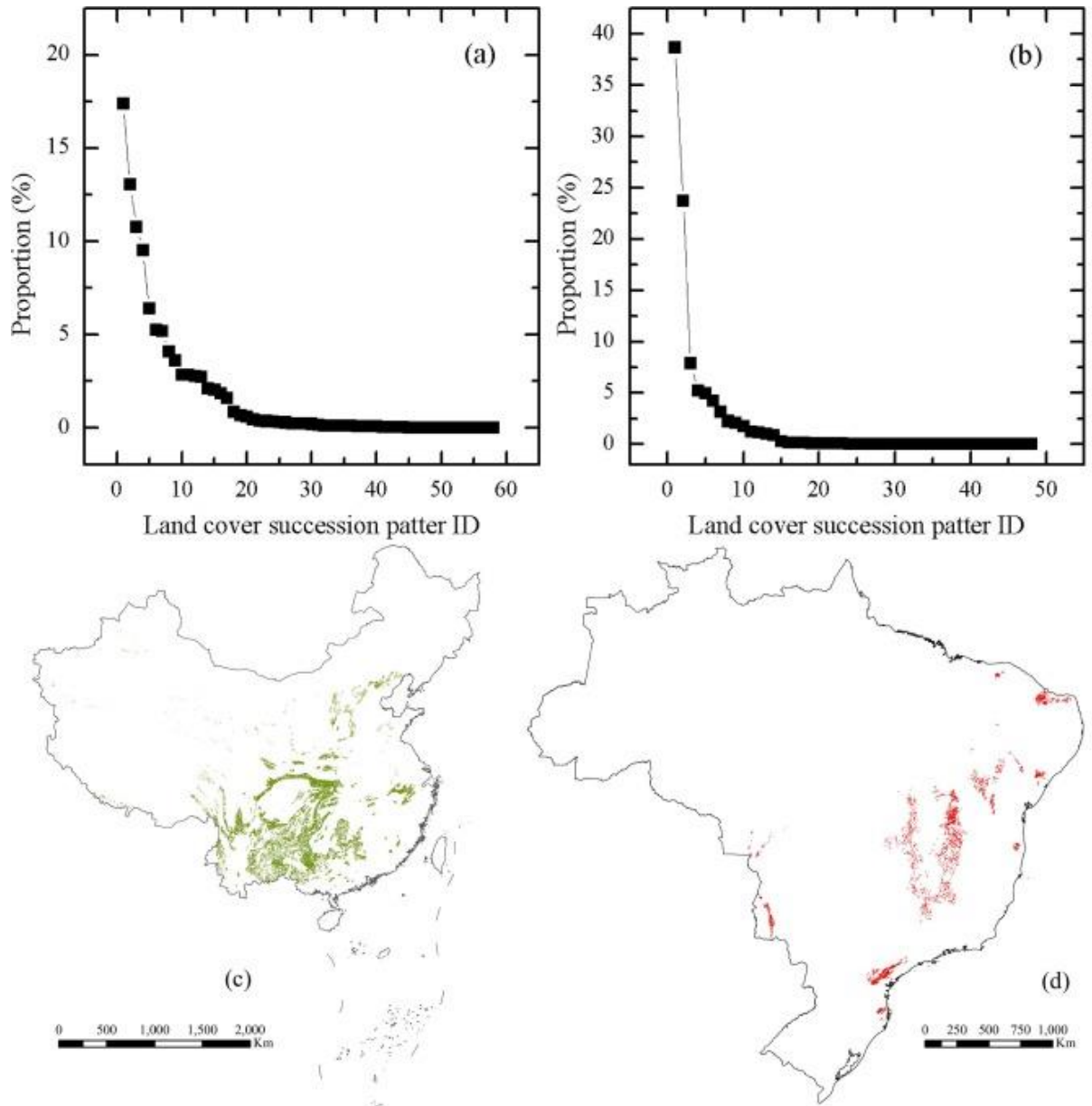


Fig. 11. Percentage of each land cover succession pattern amongst all land cover succession patterns from 2001 to 2015 in the karst areas of China (a) and Brazil (b), respectively. (c) and (d) refer to regions of grain-for-green programme in China and deforestation in Brazil, respectively. (For interpretation of the references to colour in this figure legend, the reader is referred to the web version of this article.)

#### 4. Discussion and conclusion

Karst rocky desertification has been reported in many regions including the Mediterranean European, Dinaric Karst regions of the Balkan Peninsula, over a large part of Southwest China, and most alarmingly, even in tropical rainforest areas underlain by karstic geology such as in Haiti and Barbados (Jiang et al., 2014). These changes have tremendous environmental impacts with social-economic consequences at local to national scales. It has been reported that severe soil erosion accompanied by vegetation degradation within these ecologically-fragile areas have led to bedrock exposure creating desert-like landscapes, reducing land productivity. As a result, economic development has been constrained and poverty of local communities exacerbated (Yan & Cai, 2015). Investigations of the dynamics

of global karst ecosystems and the associated driving forces are required in order to develop effective environmental protection and sustainable development strategies.

In recent years, satellite-based observations and model simulations have revealed the widespread greening of the Earth. Previous studies attributed the greening trend of global vegetated area to the dominant role of climate change (Forzieri et al., 2017; Keenan et al., 2018) in addition to the effect of anthropogenic activities (Fan et al., 2019). Nevertheless, climatic impacts on vegetation dynamics across different biomes and climate zones are contrasting (Tang et al., 2017, Chen et al., 2019a, Chen et al., 2019b, Wang et al., 2021). Forzieri et al. (2017) found that the increasing trend in leaf area index (LAI) contributed to the warming of boreal zones through a reduction of surface albedo and to an evaporation-driven cooling in arid regions. Our study has shown that vegetation changes in most global karst area were affected by precipitation, and that only relatively small area such as karst ecosystem in Canada, was dominantly influenced by temperature (Fig. 10). Climate warming was generally favorable for vegetation growth in global karst areas except those in Brazil, South Africa and Australia (Fig. S8). Increasing precipitation benefited vegetation restoration in most areas besides the northern high latitudes (Fig. S9). In the karst region of eastern Canada, temperature declines resulted in vegetation decrease, whereas increases in precipitation in Southwest China significantly contributed to ecological restoration (Brandt et al., 2018). In the karst regions of tropical Brazil, the apparent vegetation degradation was mainly driven by climatic anomalies and human disturbance (Marengo et al., 2017, Servino et al., 2018). Recently, model projections have suggested future increases in extreme climate events such as droughts and heat waves around the world (Beniston et al., 2007, Zscheischler et al., 2018), which will exert substantial pressure to the fragile karst ecosystems. The sensitivity of ecosystems to climate perturbations can be partly reduced by appropriate human management (Tong et al., 2018) but this clearly requires commitment from governments.

Vegetation monitoring from traditional optical Earth observation (EO) datasets is generally limited to the green canopy layer with less sensitivity to biomass (Tian et al., 2016, Fan et al., 2019, Huang et al., 2021). As a result, the spatial pattern and trends of productivity of global karst ecosystems remain poorly resolved. Whilst uncertainties remain in the reconstructed global continuous SIF dataset, it provides direct and spatially explicit information for quantitative monitoring of terrestrial photosynthesis and ecosystem functions across multiple spatial and temporal scales. The spatial differences in satellite-based ecosystem productivity across the globe are intrinsically determined by the climate and vegetation-related characteristics. In the tropics and subtropics, owing to favorable hydrothermal conditions, terrestrial ecosystems including forest, grassland and shrubland are green almost all year round (Fig. S1). However, a large proportion of vegetation in the mid- and high-latitudes is only active in summer and is then dormant in winter. Yu et al. (2021) stated that ecologists should not only be able to monitor dynamic changes in ecological processes, reveal mechanisms governing such processes, and quantitatively assess ecosystem responses to human activities and climate changes, but also provide accurate early warning of ecosystem changes.

Over the past few decades, intensive human pressure on land resulting from large and rapidly growing human populations has been identified as a major threat to the sustainable development of karst regions (Peng et al., 2011), especially in rural areas such as Southwest China (Yang et al., 2017a, Yang et al., 2017b). Karst regions, lying in the upper reaches of two of China's large rivers (the Yangtze and Pearl river), provide resources, in particular water, for the two most economically-developed areas in China which are located downstream in the rivers' delta regions (Bai et al., 2013), while limited conservation measures for these areas were in place during the 20th century. At the beginning of the new millennium, the State Council of China released the 'Outline of the 10th Five-year Plan of National Economical and Social Development', which clearly declared to fight against disastrous rocky desertification issues in southwestern China. Subsequently, a series of key

national ecological restoration projects including the Natural Forest Protection Project, the Grain to Green Programme, the Karst Rocky Desertification Comprehensive Control and Restoration Project and the River Shelter Forest Project were launched to restore degraded karst and other ecosystems. The year 2001 is therefore an ideal starting point with which to compare changes in China's karst environments and thereby to assess the effects of these schemes. Our results indicate that China contains one of the largest coherent karst regions and accounts for 43.66% of the observed total net change in global SIF between 2001 and 2016 (Table 1, Fig. 7). These findings corroborate other recent studies that have suggested that implementation of the afforestation and reforestation projects during this period has significantly increased vegetation growth and ecosystem carbon sequestration for mitigating global climate change (Lu et al., 2018, Tong et al., 2018). In addition, this study found that except China, the EU, Russia, Canada, the USA and several Southeast Asia countries also made positive contributions.

Within South America, karst landscapes cover 2% of the land area (370, 809 km<sup>2</sup>), the majority of which is in Brazil and comprises woody savanna from open grasslands to forests. Despite a persistent and widespread increase in SIF for global karst ecosystems, this study found that approximately 19.43% of the karst area in Brazil was subject to serious vegetation degeneration over the period 2001–2016. As a result, Brazil makes a negative contribution to global greening of karstic environments (Fig. 7, Table 1). Currently, Brazil has become a global agricultural leader in the production of commodity raw crops such as soybean, sugarcane, cotton, and corn (Zalles et al., 2019). These crops often have short growth periods constraining their contribution to ecosystem productivity. Meanwhile, the carbon uptake by crops during their growth will be released to the atmosphere after much shorter periods compared to the forests that they often replace (West et al., 2010). Despite several strategic conservation measures to reverse deforestation (Nepstad et al., 2014), the rate of forest removal remains high in Brazil, endangering the long-term sustainability of the country and the global climate system (Schielein and Börner, 2018). Fig. 11 showed that the proportion of forest area declined over the study period. Artaxo (2019) reported that Amazonian forest, including in those areas underlain by karstic geology, is now suffering from losses at an accelerated rate through human-lit fires for agriculture. A recent study (Matricardi et al., 2020) also revealed that long-term forest degradation even surpassed deforestation in the Brazilian Amazon. Chen et al., 2019a, Chen et al., 2019b reported the leading and impressive changes in agricultural production in Brazil, but the greening from croplands is nearly offset by the browning of forest. Besides, this study revealed that many countries in East Africa such as Tanzania, Mozambique, Madagascar and South Africa are experiencing browning in the past decades. Therefore, irrational land use and forest cutting could result in serious land degradation, and the decrease of vegetation productivity. It is crucial for a global joint action on karst environmental protection, otherwise gains in one area can be easily offset by loss in other areas. These analyses have immediate implications for societal grand challenges in relation to climate change mitigation as formulated by the UN Sustainable Development Goals.

Our study found that these satellite-derived products were easy to characterize spatial differences in vegetation productivity across global karst ecosystems (Fig. 1, Fig. 2). However, contrasting performances were revealed when such products aimed to capture interannual or long-term dynamics, just like Fig. 5, Fig. 6 showed that these remote sensing variables exhibited significantly different trends both globally and in different countries. Compared with the MODIS GPP product, the SIF observations indirectly confirmed the better performance of the VPM GPP results (Chen et al., 2019a, Chen et al., 2019b). It can be ascribed to an improved light use efficiency parameter with the separate treatment for C<sub>3</sub>/C<sub>4</sub> photosynthesis pathways in the VPM model. Thus, the knowledge derived from the global assessment herein can improve our understanding of both global and regional ecosystem dynamics. Meanwhile, appropriate ecosystem management can help to ensure regional ecological security and sustainable development. Nevertheless, it is necessary to take into account the country's own level of socio-economic development and the difficulty of

restoring karst areas in the region. This forms an important foundation for a better management of karst ecosystems that include an effective mitigation of vegetation degradation.

## Acknowledgments

This study was jointly supported by the Special Project on National Science and Technology Basic Resources Investigation of China (Grant No. 2021FY100701) and the National Major Projects on High-Resolution Earth Observation System (Grant No. 21-Y20B01-9001-19/22). We would like to express our gratitude to all the scientists that have contributed to these multi-source datasets used in the study that includes the global OCO-2 SIF data set (GOSIF), VPM GPP and MODIS GPP products, the Climate Change Initiative Land Cover (CCI-LC) products (v2) and the meteorological data from the Global Land Assimilation System (GLDAS-2.1).

All data used in this study are publicly available. GOSIF data is available at [http://data.globalecology.unh.edu/data/GOSIF\\_v2/](http://data.globalecology.unh.edu/data/GOSIF_v2/). MODIS GPP is available at <http://www.nts.gov.umt.edu/project/mod17>. VPM GPP can be downloaded from <https://doi.org/10.6084/m9.figshare.c.3789814>. CCI-LC products are available at <http://maps.elie.ucl.ac.be/CCI/viewer/download.php>. The meteorological data from the Global Land Assimilation System (GLDAS-2.1) can be downloaded via <http://disc.sci.gsfc.nasa.gov/uui/datasets?keywords=GLDAS>. The data on global country administrative areas (GADM V3.6) is available at <https://gadm.org/data.html>. The karst boundary is based on the World Map of Carbonate Rock Outcrops (V3.0) from the website [https://www.fos.auckland.ac.nz/our\\_research/karst/](https://www.fos.auckland.ac.nz/our_research/karst/).

## Author contributions

X.T. and C.W. designed the research. X.T. analyzed the data and wrote the paper. J.X., H.Y., Y.Z. and C.W. provided comments and suggestions. X.L., Z.D. and J.H. helped to process the data. M.M., P.Y., Q.G., H.Y. and J.R.T. provided valuable discussions and extensively revised the writing. All authors contributed ideas for analyses, comments and critiques.

## References

- Artaxo, P., 2019. Working together for Amazonia. *Science* 363 (6425), 323.
- Bai, X.-Y., Wang, S.-J., Xiong, K.-N., 2013. Assessing spatial-temporal evolution processes of karst rocky desertification land: indications for restoration strategies. *Land Degrad. Dev.* 24 (1), 47–56.
- Beniston, M., Stephenson, D.B., Christensen, O.B., Ferro, C.A.T., Frei, C., Goyette, S., Halsnaes, K., Holt, T., Jylhä, K., Koffi, B., Palutikof, J., Schöll, R., Semmler, T., Woth, K., 2007. Future extreme events in European climate: an exploration of regional climate model projections. *Clim. Change* 81 (S1), 71–95.
- Brandt, M., Yue, Y., Wigneron, J.P., Tong, X., Tian, F., Jepsen, M.R., Xiao, X., Verger, A., Mialon, A., Al-Yaari, A., Wang, K., Fensholt, R., 2018. Satellite-observed major greening and biomass increase in south China karst during recent decade. *Earth's Future* 6 (7), 1017–1028.
- Chen, Y., Gu, H., Wang, M., Gu, Q., Ding, Z., Ma, M., Liu, R., Tang, X., 2019b. Contrasting performance of the remotely-derived GPP products over different climate zones across China. *Remote Sensing* 11 (16), 1855. <https://doi.org/10.3390/rs11161855>.

- Chen, C., Park, T., Wang, X., Piao, S., Xu, B., Chaturvedi, R.K., Fuchs, R., Brovkin, V., Ciais, P., Fensholt, R., Tømmervik, H., Bala, G., Zhu, Z., Nemani, R.R., Myneni, R.B., 2019a. China and India lead in greening of the world through land-use management. *Nat. Sustainability* 2 (2), 122–129.
- De Waele, J., Gutierrez, F., Audra, P., 2015. Karst geomorphology: from hydrological functioning to palaeoenvironmental reconstructions. Part II. *Geomorphology* 247, 1–1.
- Fan, L., Wigneron, J.-P., Ciais, P., Chave, J., Brandt, M., Fensholt, R., Saatchi, S.S., Bastos, A., Al-Yaari, A., Hufkens, K., Qin, Y., Xiao, X., Chen, C., Myneni, R.B., Fernandez-Moran, R., Mialon, A., Rodriguez-Fernandez, N.J., Kerr, Y., Tian, F., Peñuelas, J., 2019. Satellite-observed pantropical carbon dynamics. *Nat. Plants* 5 (9), 944–951.
- Fensholt, R., Langanke, T., Rasmussen, K., Reenberg, A., Prince, S.D., Tucker, C., Scholes, R.J., Le, Q.B., Bondeau, A., Eastman, R., Epstein, H., Gaughan, A.E., Hellden, U., Mbow, C., Olsson, L., Paruelo, J., Schweitzer, C., Seaquist, J., Wessels, K., 2012. Greenness in semi-arid areas across the globe 1981–2007—an Earth Observing Satellite based analysis of trends and drivers. *Remote Sens. Environ.* 121, 144–158.
- Ford, D., Williams, P.D., 2007. *Karst Hydrogeology and Geomorphology*. John Wiley & Sons.
- Forzieri, G., Alkama, R., Miralles, D.G., Cescatti, A., 2017. Satellites reveal contrasting responses of regional climate to the widespread greening of Earth. *Science* 356 (6343), 1180–1184.
- Gocic, M., Trajkovic, S., 2013. Analysis of changes in meteorological variables using Mann-Kendall and Sen's slope estimator statistical tests in Serbia. *Global Planet. Change* 100, 172–182.
- Grimm, N.B., Chapin, F.S., Bierwagen, B., Gonzalez, P., Groffman, P.M., Luo, Y., Melton, F., Nadelhoffer, K., Pairis, A., Raymond, P.A., Schimel, J., Williamson, C.E., 2013. The impacts of climate change on ecosystem structure and function. *Front. Ecol. Environ.* 11 (9), 474–482.
- Guanter, L., Zhang, Y., Jung, M., Joiner, J., Voigt, M., Berry, J.A., Frankenberg, C., Huete, A.R., Zarco-Tejada, P., Lee, J.-E., Moran, M.S., Ponce-Campos, G., Beer, C., Camps-Valls, G., Buchmann, N., Gianelle, D., Klumpp, K., Cescatti, A., Baker, J.M., Griffis, T.J., 2014. Global and time-resolved monitoring of crop photosynthesis with chlorophyll fluorescence. *Proc. Natl. Acad. Sci.* 111 (14), E1327–E1333.
- Hiroko, B., Rodell, M., 2016. GLDAS Noah Land Surface Model L4 Monthly 0.25 x 0.25 degree V2.1. NASA.
- Huang, J., Ge, Z., Huang, Y., Tang, X., Shi, Z., Lai, P., et al., 2021. Climate change and ecological engineering jointly induced vegetation greening in global karst regions from 2001 to 2020. *Plant Soil*, 1–20.
- Jiang, Z., Lian, Y., Qin, X., 2014. Rocky desertification in Southwest China: impacts, causes, and restoration. *Earth Sci. Rev.* 132, 1–12.
- Ju, J., Masek, J.G., 2016. The vegetation greenness trend in Canada and US Alaska from 1984–2012 Landsat data. *Remote Sens. Environ.* 176, 1–16.
- Keenan, T.F., Riley, W.J., 2018. Greening of the land surface in the world's cold regions consistent with recent warming. *Nat. Clim. Change* 8 (9), 825–828.
- Laffoon, M., Meier, A., Groves, C., 2015. Potential Application of Hugelkultur to Increase Water Holding Capacity of Karst Rocky Desertified Land.

- Li, X., Xiao, J., 2019. A global, 0.05-degree product of solar-induced chlorophyll fluorescence derived from OCO-2, MODIS, and reanalysis data. *Remote Sensing* 11 (5), 517.
- Li, X., Xiao, J., He, B., Altaf Arain, M., Beringer, J., Desai, A.R., Emmel, C., Hollinger, D. Y., Krasnova, A., Mammarella, I., Noe, S.M., Ortiz, P.S., Rey-Sanchez, A.C., Rocha, A. V., Varlagin, A., 2018. Solar-induced chlorophyll fluorescence is strongly correlated with terrestrial photosynthesis for a wide variety of biomes: First global analysis based on OCO-2 and flux tower observations. *Glob. Change Biol.* 24 (9), 3990–4008.
- Lu, F., Hu, H., Sun, W., Zhu, J., Liu, G., Zhou, W., Zhang, Q., Shi, P., Liu, X., Wu, X., Zhang, L.u., Wei, X., Dai, L., Zhang, K., Sun, Y., Xue, S., Zhang, W., Xiong, D., Deng, L., Liu, B., Zhou, L.i., Zhang, C., Zheng, X., Cao, J., Huang, Y., He, N., Zhou, G., Bai, Y., Xie, Z., Tang, Z., Wu, B., Fang, J., Liu, G., Yu, G., 2018. Effects of national ecological restoration projects on carbon sequestration in China from 2001 to 2010. *Proc. Natl. Acad. Sci.* 115 (16), 4039–4044.
- Magney, T.S., Bowling, D.R., Logan, B.A., Grossmann, K., Stutz, J., Blanken, P.D., et al., 2019. Mechanistic evidence for tracking the seasonality of photosynthesis with solar- induced fluorescence. *Proc. Natl. Acad. Sci.* 116 (24), 11640–11645.
- Mao, J., Ribes, A., Yan, B., Shi, X., Thornton, P.E., Séférian, R., Ciais, P., Myneni, R.B., Douville, H., Piao, S., Zhu, Z., Dickinson, R.E., Dai, Y., Ricciuto, D.M., Jin, M., Hoffman, F.M., Wang, B., Huang, M., Lian, X.u., 2016. Human-induced greening of the northern extratropical land surface. *Nat. Clim. Change* 6 (10), 959–963.
- Marengo, J.A., Torres, R.R., Alves, L.M., 2017. Drought in Northeast Brazil—past, present, and future. *Theor. Appl. Climatol.* 129 (3-4), 1189–1200.
- Matricardi, E.A.T., Skole, D.L., Costa, O.B., Pedlowski, M.A., Samek, J.H., Miguel, E.P., 2020. Long-term forest degradation surpasses deforestation in the Brazilian Amazon. *Science* 369 (6509), 1378–1382.
- Nepstad, D., McGrath, D., Stickler, C., Alencar, A., Azevedo, A., Swette, B., et al., 2014. Slowing Amazon deforestation through public policy and interventions in beef and soy supply chains. *Science* 344 (6188), 1118–1123.
- Peng, J., Xu, Y., Cai, Y., Xiao, H., 2011. Climatic and anthropogenic drivers of land use/cover change in fragile karst areas of southwest China since the early 1970s: a case study on the Maotiaohe watershed. *Environ. Earth Sci.* 64 (8), 2107–2118.
- Piao, S., Yin, G., Tan, J., Cheng, L., Huang, M., Li, Y., et al., 2015. Detection and attribution of vegetation greening trend in China over the last 30 years. *Glob. Change Biol.* 21 (4), 1601–1609.
- Poulter, B., MacBean, N., Hartley, A., Khlystova, I., Arino, O., Betts, R., Bontemps, S., Boettcher, M., Brockmann, C., Defourny, P., Hagemann, S., Herold, M., Kirches, G., Lamarche, C., Lederer, D., Ottlé, C., Peters, M., Peylin, P., 2015. Plant functional type classification for earth system models: results from the European Space Agency's Land Cover Climate Change Initiative. *Geosci. Model Dev.* 8 (7), 2315–2328.
- Schielein, J., Börner, J., 2018. Recent transformations of land-use and land-cover dynamics across different deforestation frontiers in the Brazilian Amazon. *Land Use Policy* 76, 81–94.
- Servino, R.N., Gomes, L.E.d.O., Bernardino, A.F., 2018. Extreme weather impacts on tropical mangrove forests in the Eastern Brazil Marine Ecoregion. *Sci. Total Environ.* 628-629, 233–240.

- Sun, Y., Frankenberg, C., Wood, J.D., Schimel, D.S., Jung, M., Guanter, L., Drewry, D.T., Verma, M., Porcar-Castell, A., Griffis, T.J., Gu, L., Magney, T.S., Köhler, P., Evans, B., Yuen, K., 2017. OCO-2 advances photosynthesis observation from space via solar-induced chlorophyll fluorescence. *Science* 358 (6360). <https://doi.org/10.1126/science.aam5747>.
- Tang, X., Li, H., Desai, A.R., Nagy, Z., Luo, J., Kolb, T.E., et al., 2014. How is water-use efficiency of terrestrial ecosystems distributed and changing on Earth? *Sci. Rep.* 4 (1), 1–11.
- Tang, X., Li, H., Ma, M., Yao, L.i., Peichl, M., Arain, A., Xu, X., Goulden, M., 2017. How do disturbances and climate effects on carbon and water fluxes differ between multi-aged and even-aged coniferous forests? *Sci. Total Environ.* 599-600, 1583–1597.
- Tian, F., Brandt, M., Liu, Y.Y., Verger, A., Tagesson, T., Diouf, A.A., Rasmussen, K., Mbow, C., Wang, Y., Fensholt, R., 2016. Remote sensing of vegetation dynamics in drylands: Evaluating vegetation optical depth (VOD) using AVHRR NDVI and in situ green biomass data over West African Sahel. *Remote Sens. Environ.* 177, 265–276.
- Tong, X., Brandt, M., Yue, Y., Horion, S., Wang, K., Keersmaecker, W.D., Tian, F., Schurgers, G., Xiao, X., Luo, Y., Chen, C., Myneni, R., Shi, Z., Chen, H., Fensholt, R., 2018. Increased vegetation growth and carbon stock in China karst via ecological engineering. *Nat. Sustainability* 1 (1), 44–50.
- Walther, S., Voigt, M., Thum, T., Gonsamo, A., Zhang, Y., Köhler, P., Jung, M., Varlagin, A., Guanter, L., 2016. Satellite chlorophyll fluorescence measurements reveal large-scale decoupling of photosynthesis and greenness dynamics in boreal evergreen forests. *Glob. Change Biol.* 22 (9), 2979–2996.
- Wang, M., Ding, Z., Wu, C., Song, L., Ma, M., Yu, P., Lu, B., Tang, X., 2021. Divergent responses of ecosystem water-use efficiency to extreme seasonal droughts in Southwest China. *Sci. Total Environ.* 760, 143427. <https://doi.org/10.1016/j.scitotenv.2020.143427>.
- Wang, X., Xiao, J., Li, X., Cheng, G., Ma, M., Zhu, G., Altaf Arain, M., Andrew Black, T., Jassal, R.S., 2019. No trends in spring and autumn phenology during the global warming hiatus. *Nat. Commun.* 10 (1) <https://doi.org/10.1038/s41467-019-10235-8>.
- West, P.C., Gibbs, H.K., Monfreda, C., Wagner, J., Barford, C.C., Carpenter, S.R., Foley, J. A., 2010. Trading carbon for food: Global comparison of carbon stocks vs. crop yields on agricultural land. *Proc. Natl. Acad. Sci.* 107 (46), 19645–19648.
- Wu, X., Xiao, X., Zhang, Y., He, W., Wolf, S., Chen, J., He, M., Gough, C.M., Qin, Y., Zhou, Y., Doughty, R., Blanken, P.D., 2018. Spatiotemporal consistency of four gross primary production products and solar-induced chlorophyll fluorescence in response to climate extremes across CONUS in 2012. *J. Geophys. Res. Biogeosci.* 123 (10), 3140–3161.
- Yan, X., Cai, Y.L., 2015. Multi-scale anthropogenic driving forces of karst rocky desertification in Southwest China. *Land Degrad. Dev.* 26 (2), 193–200.
- Yang, H., Ma, M., Flower, R.J., Thompson, J.R., Ge, W., 2017a. Preserve Precambrian fossil heritage from mining. *Nat. Ecol. Evol.* 1 (8), 1048–1049.
- Yang, Y., Xiao, P., Feng, X., Li, H., 2017b. Accuracy assessment of seven global land cover datasets over China. *ISPRS J. Photogramm. Remote Sens.* 125, 156–173.
- Yang, P., Wang, Y., Wu, X., Chang, L., Ham, B., Song, L., Groves, C., 2020. Nitrate

- sources and biogeochemical processes in karst underground rivers impacted by different anthropogenic input characteristics. *Environ. Pollut.* 265, 114835.
- Yu, G., Piao, S., Zhang, Y., Liu, L., Peng, J., Niu, S., 2021. Moving toward a new era of ecosystem science. *Geogr. Sustainability* 2 (3), 151–162.
- Zalles, V., Hansen, M.C., Potapov, P.V., Stehman, S.V., Tyukavina, A., Pickens, A., Song, X.-P., Adusei, B., Okpa, C., Aguilar, R., John, N., Chavez, S., 2019. Near doubling of Brazil's intensive row crop area since 2000. *Proc. Natl. Acad. Sci.* 116 (2), 428–435.